PROCEEDINGS OF SCIENCE

Vector Mesons at H1

Niklaus Berger*
Institute for Particle Physics, ETH Zurich, 8093 Zurich, Switzerland
E-mail: nberger@phys.ethz.ch

on behalf of the H1 collaboration

The study of exclusive vector meson production at HERA sheds light on the nature of diffractive exchanges. H1 has performed the first measurement of the pomeron trajectory in ρ^0 photoproduction with data from a single experiment. The result is $\alpha_{I\!P}(t) = 1.093 \pm 0.003(stat.)^{+0.008}_{-0.007}(syst.) + (0.116 \pm 0.027(stat.)^{+0.036}_{-0.046}(syst.))\mathrm{GeV}^{-2} \cdot t$. An analysis of ρ^0 photoproduction at high $|t|$ shows significant evidence for *s*-channel helicity *non*-conservation. Cross-sections for J/ψ photo- and electroproduction were measured over a wide kinematic range and are found to be sensitive to the gluon density in the proton.

DIFFRACTION 2006 - International Workshop on Diffraction in High-Energy Physics
September 5-10 2006
Adamantas, Milos island, Greece

*Speaker.

PoS(DIFF2006)011

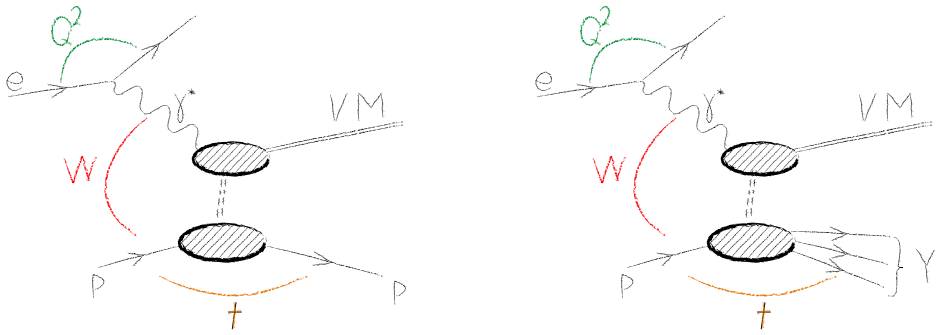

Figure 1: Schematic representation of elastic (left) and proton dissociative (right) vector meson production. The main kinematic quantities are the virtuality of the exchanged photon Q^2, the photon-proton center-of-mass energy W, the squared four-momentum transfer at the proton vertex t, the mass of the produced vector meson M_{VM} and the mass of the proton dissociative system M_Y.

1. Introduction

Quantum Chromodynamics (QCD) describes the strong force between hadrons and between their constituents, the quarks and gluons. QCD is very successful in the limit of short distances ("hard" interactions), where perturbative methods (pQCD) are applicable. Hadron scattering cross-sections are however dominated by long-range forces ("soft" interactions), where an understanding in the framework of QCD remains a challenge. A large fraction of these soft interactions are mediated by a colourless exchange ("diffractive" interactions). In Regge theory, diffractive interactions are well described by the t-channel exchange of a trajectory with vacuum quantum numbers called "pomeron". In the high energy limit, the Pomeron exchange dominates and leads to an almost energy-independent total cross-section.

The production of vector mesons (see Figure 1) is an example of a diffractive process with a clearly defined experimental signature. The wide range in the γp center of mass energy $W_{\gamma p}$ and the negative squared four-momentum transfer at the electron vertex Q^2 make the HERA electron-proton[1] collider and its two colliding beam experiments H1 and ZEUS a unique facility to study the nature of diffractive processes and especially the transition region between soft and hard regimes.

In the following, three recent H1 analyses on vector meson production are presented. New preliminary results on ρ^0 production at low $|t|$ are described in detail, whilst for the published analyses of J/ψ production [1] and ρ^0 production at high $|t|$ [2], the main results are summarised.

2. Diffractive ρ^0 photoproduction

In 2002, the HERA collider has been upgraded to provide higher luminosity. For the HERA II era, the H1 detector was equipped with a new Fast Track Trigger (FTT [3, 4, 5]). This new device recognises and counts tracks in the Central Jet Chamber (CJC) down to 100 MeV transverse momentum and is thus ideally suited to trigger on diffractively produced vector mesons. In a three month period in 2005 with stable trigger and chamber settings more than 240'000 ρ^0 candidate events were recorded; the luminosity corrected for prescales amounts to 570 nb^{-1}.

[1] HERA can be operated with both electrons and positrons - in the following, electron is always used to refer to both.

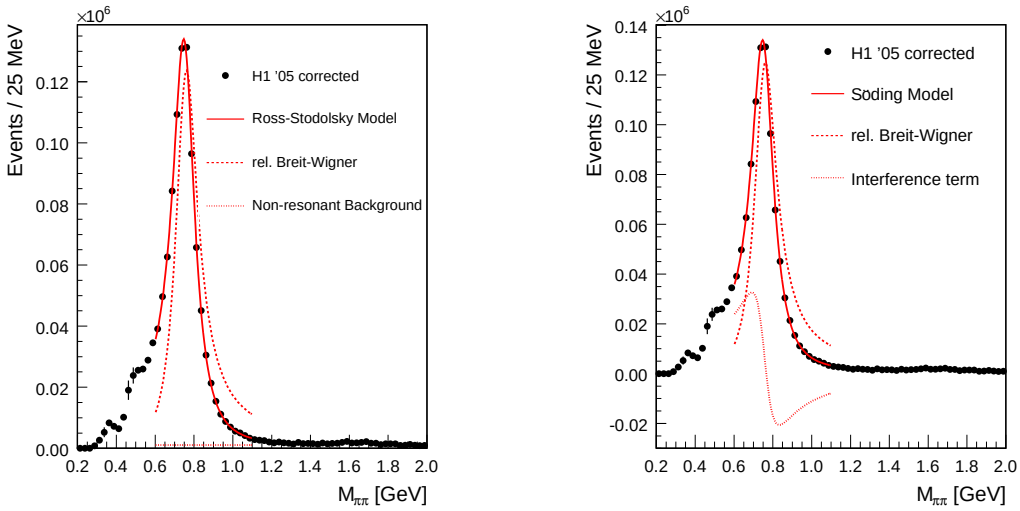

Figure 2: Di-pion mass spectrum corrected for acceptance and detector effects. The ρ^0 peak is fitted with a skewed relativistic Breit-Wigner as proposed by M. Ross and L. Stodolsky [6] (left) and with a relativistic Breit-Wigner supplemented by an interference term as proposed by P. Söding [7] (right).

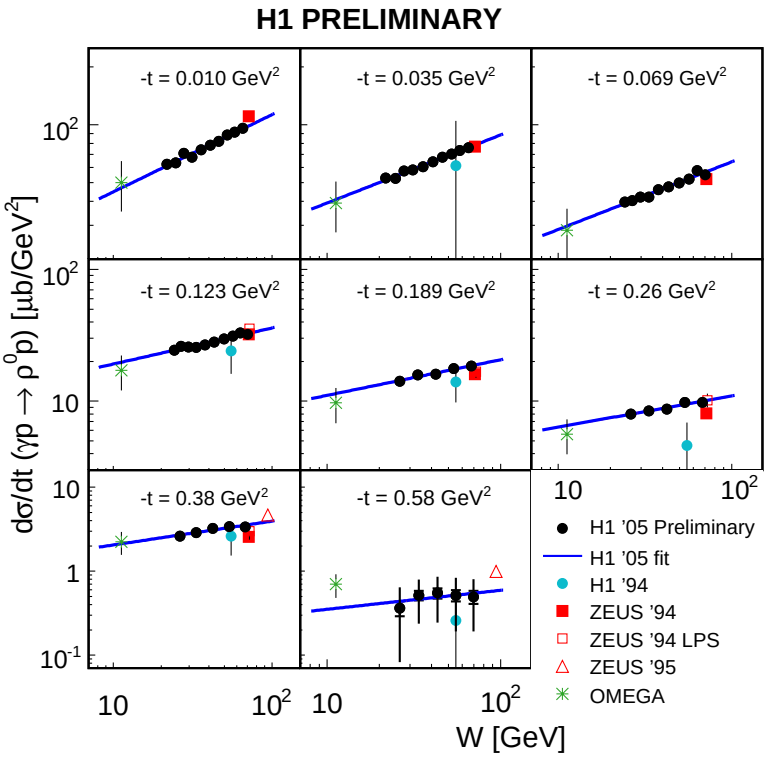

Figure 3: Cross-sections for elastic ρ^0 production versus W in eight bins of t. The preliminary H1 results are compared to measurements by the ZEUS [8, 9, 10] and OMEGA collaborations [11] as well as to previous H1 results [12].

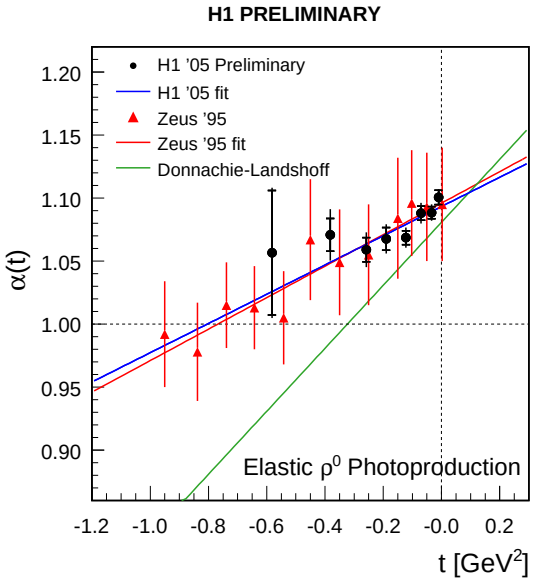

Figure 4: Pomeron trajectory for elastic ρ^0 production. The preliminary H1 measurement is compared to the combined ZEUS-OMEGA-H1 result [10] and to the trajectory obtained in a global fit to hadronic cross-sections by Donnachie and Landshoff [13, 14, 15].

ρ^0 candidate events were selected by the following criteria:

- A reconstructed primary vertex within 25 cm of the nominal interaction point along the beam axis,
- Exactly two well-measured primary vertex fitted tracks with a $p_\perp > 200$ MeV and a polar angle ϑ between 20° and 160° (where $\vartheta = 0°$ corresponds to proton beam direction),
- No additional tracks in the central or forward tracker,
- No calorimeter cluster with an energy above noise level not associated to one of the tracks,
- No scattered electron candidate.

The events thus selected are distributed in 80 bins in W and t; there are twelve bins in t, in turn subdivided into 10 ($|t| < 0.16$ GeV^2) or 5 ($|t| > 0.16$ GeV^2) bins in W. Within each of these bins, the invariant mass spectrum under a charged pion hypothesis was reconstructed from the momenta of the two tracks. These spectra were then corrected for acceptance, detector- and trigger efficiency using the DIFFVM Monte Carlo generator [16] – for more details on the analysis, see [17]. The resulting mass distribution, integrated over all bins, is shown in Figure 2. Due to the large width of the ρ^0 resonance, there is significant interference between ρ^0 production with a subsequent decay to two pions and non-resonant di-pion production. This interference leads to a distortion of the observed ρ^0-peak. Two models have been put forward to describe this distortion: The ansatz by P. Söding [7] describes the shape by a relativistic Breit-Wigner, a term for the non-resonant

production (here taken to be constant), and an interference term:

$$\frac{\mathrm{d}N}{\mathrm{d}m_{\pi\pi}} = \frac{N_0 m_\rho \Gamma_\rho m_{\pi\pi} + I(m_\rho^2 - m_{\pi\pi}^2)}{(m_\rho^2 - m_{\pi\pi}^2)^2 + m_\rho^2 \Gamma_\rho^2} + B,$$

where N_0, I and B parametrise the contributions from resonant ρ_0 production, interference and background, respectively. m_ρ is the nominal ρ_0 mass and

$$\Gamma_\rho = \Gamma_{\rho,0} \left(\frac{m_{\pi\pi}^2 - 4m_\pi^2}{m_\rho^2 - 4m_\pi^2} \right)^{\frac{3}{2}} \frac{m_\rho}{m_{\pi\pi}}$$

the mass dependent width ($\Gamma_{\rho,0}$ is the nominal width) following the suggestion of J.D. Jackson [18]. In the ansatz by M. Ross and L. Stodolsky [6], the relativistic Breit-Wigner is multiplied by a skewing term:

$$\frac{\mathrm{d}N}{\mathrm{d}m_{\pi\pi}} = \frac{N_0 m_\rho \Gamma_\rho m_{\pi\pi}}{(m_\rho^2 - m_{\pi\pi}^2)^2 + m_\rho^2 \Gamma_\rho^2} \left(\frac{m_\rho}{m_{\pi\pi}} \right)^n + B,$$

where n is the skewing parameter. Both models are used to fit the invariant mass distributions and extract the number of resonantly produced ρ^0s (by integrating the relativistic Breit-Wigner from $2m_\pi$ to $m_\rho + 5\Gamma_{\rho,0} = 1.52$ GeV) in each bin. The two fit methods yield compatible results. To obtain the photoproduction cross-section, the ep cross-section is divided by the photon flux integrated over the respective W range and up to $Q^2 = 4$ GeV^2.

The following sources of background where investigated: ϕ, ω, $\rho(1450)$ and $\rho(1700)$ meson production as well as ρ^0 production outside the signal region of $Q^2 < 4$ GeV^2 and $(M_Y^2 + Q^2)/(W^2 + Q^2) < 0.01$. While the contributions from other mesons were found to be below 2% (a corresponding normalisation uncertainty is assigned to the result), the contributions from outside the signal region were absorbed into the reconstruction efficiency using the Monte Carlo simulation.

To separate the elastic events from those where the proton dissociates diffractively into a state of mass M_Y, the Forward Muon Detector (FMD) and the Forward Tagging System (FTS) of H1 were used to detect secondary particles created by interactions of the proton dissociative state with the beam pipe. The tagging efficiency was determined from the simulation, whilst the noise in these detectors was determined from the data. An unfolding procedure was then applied to extract the number of elastic and dissociative events from the measured number of events with and without signals in the forward detectors.

The resulting elastic cross-sections are shown in Figure 3. For every t range, the cross-sections are then fitted to the form

$$\frac{\mathrm{d}\sigma_{\gamma p}(W)}{\mathrm{d}t} = \frac{\mathrm{d}\sigma_{\gamma p}(W_0)}{\mathrm{d}t} \left(\frac{W}{W_0} \right)^{4(\alpha-1)}$$

with $W_0 = 37$ GeV. The value of α is the value of the pomeron trajectory $\alpha = \alpha_{\mathbb{P}}(t)$. The resulting trajectory is shown in Figure 4. A linear fit gives

$$\alpha_{\mathbb{P}}(t) = 1.093 \pm 0.003(stat.)^{+0.008}_{-0.007}(syst.) + (0.116 \pm 0.027(stat.)^{+0.036}_{-0.056}(syst.))\mathrm{GeV}^{-2} \cdot t.$$

This result is in agreement with a previous measurement by the ZEUS collaboration [10]:

$$\alpha_{\mathbb{P}}(t) = 1.096 \pm 0.021 + (0.125 \pm 0.038)\mathrm{GeV}^{-2} \cdot t.$$

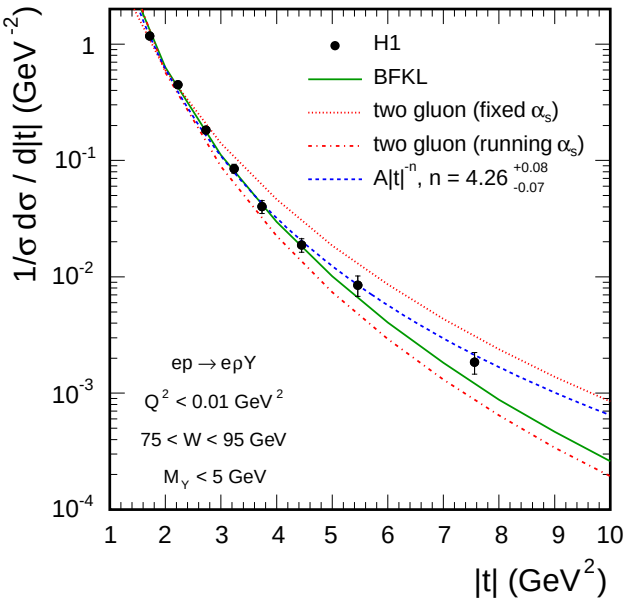

Figure 5: The t spectrum for ρ^0 production compared to two-gluon models and a BFKL based model [19, 20].

and indicates that the pomeron trajectory, as observed in elastic ρ^0 photoproduction, has a significantly smaller slope than the value of $\alpha'_{\mathbb{P}} = 0.25$ GeV^{-2} derived [14, 15] from other hadron scattering data.

3. Diffractive ρ^0 photoproduction at high $|t|$

An H1 analysis of ρ^0 photoproduction at high $|t|$ ($1.5 < |t| < 10$ GeV^2) [2] using HERA I data has been recently published. The results are compared to two-gluon models and a leading logarithm BFKL calculation [19, 20]. The $|t|$ dependence of the cross-section shown in Figure 5 is well described by a power law dependence $\mathrm{d}\sigma/\mathrm{d}|t| \propto |t|^{-n}$, where $n = 4.26 \pm 0.06$ (stat.)$^{+0.06}_{-0.04}$ (syst.). In contrast to the two-gluon models, the BFKL based model describes the data well.

The study of the helicity properties of vector meson production provides additional insights into the nature of the diffractive exchange. In the vector meson dominance model, s-channel helicity conservation (SCHC) holds, i.e. the vector meson retains the helicity of the incoming photon. pQCD based models on the other hand predict non-vanishing amplitudes for helicity flips. In principle, three helicity angles can be measured (see Figure 6). As the scattered electron is not detected, the angle Φ is not accessible in photoproduction. Integrating over Φ, the cross-section depends on the spin-density matrix elements r^{04}_{00}, $\mathrm{Re}[r^{04}_{10}]$ and r^{04}_{1-1} as follows

$$\frac{1}{\sigma}\frac{\mathrm{d}^2\sigma}{\mathrm{d}\cos\theta^*\mathrm{d}\phi^*} = \frac{3}{4\pi}\left(\frac{1}{2}(1-r^{04}_{00}) + \frac{1}{2}(3r^{04}_{00}-1)\cos^2\theta^* - \sqrt{2}\mathrm{Re}[r^{04}_{10}]\sin 2\theta^*\cos\phi^* - r^{04}_{1-1}\sin^2\theta^*\cos 2\phi^*\right).$$

The spin density matrix elements can thus be extracted by a two-dimensional fit to the helicity angle distributions (see Figure 7). The results are compatible with the previous measurements by

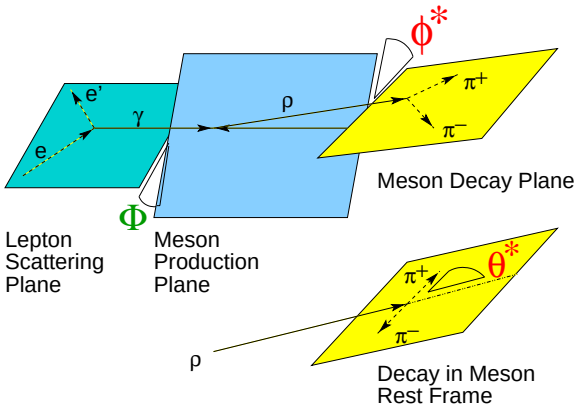

Figure 6: Illustration of the helicity angles Φ (not accessible in photoproduction), ϕ^* and θ^*.

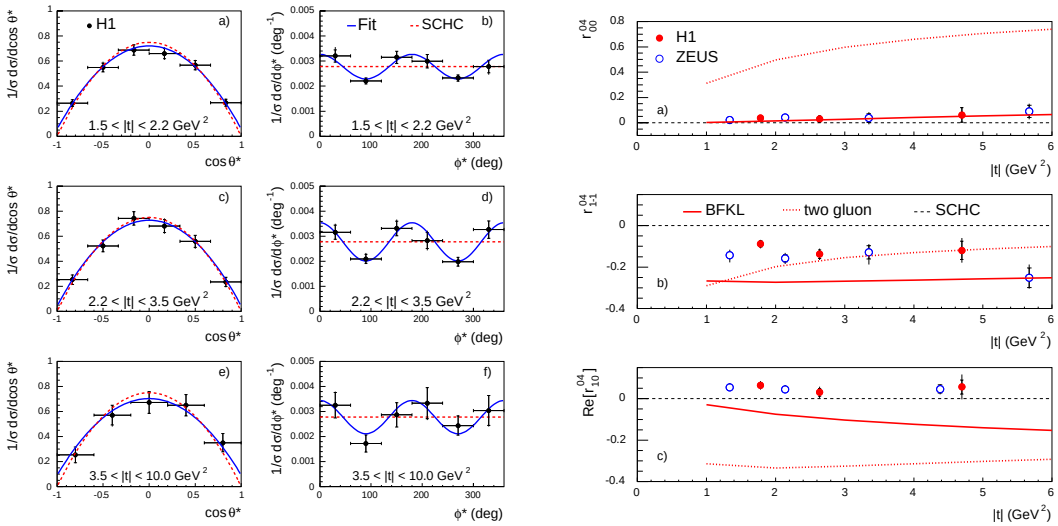

Figure 7: Angular distributions for ρ^0 photoproduction (left). The red dashed line shows the expectation for *s*-channel helicity conservation (SCHC) and the blue continuos line shows the projection of the 2-dimensional fit described in the text. The spin density matrix elements thus obtained are shown on the right and compared to the ZEUS measurement [21], the expectation for SCHC and the expectations from a two-gluon and a BFKL based model [19, 20].

ZEUS [21] and show that SCHC is violated. The two-gluon model does not describe the measurement, whereas the BFKL model correctly predicts the $|t|$ dependence of r^{04}_{00}, overestimates the magnitude of r^{04}_{1-1} and predicts the wrong sign for $\mathrm{Re}[r^{04}_{10}]$.

4. J/ψ photo- and electroproduction

The elastic production of J/ψ mesons was studied in [1]. Effective pomeron trajectories were determined for photo- and electroproduction and are shown in Figure 8. The result for photoproduction is

$$\alpha_{I\!P}(t) = 1.224 \pm 0.010(stat.) \pm 0.012(syst.) + (0.164 \pm 0.028(stat.) \pm 0.030(syst.))\mathrm{GeV}^{-2} \cdot t$$

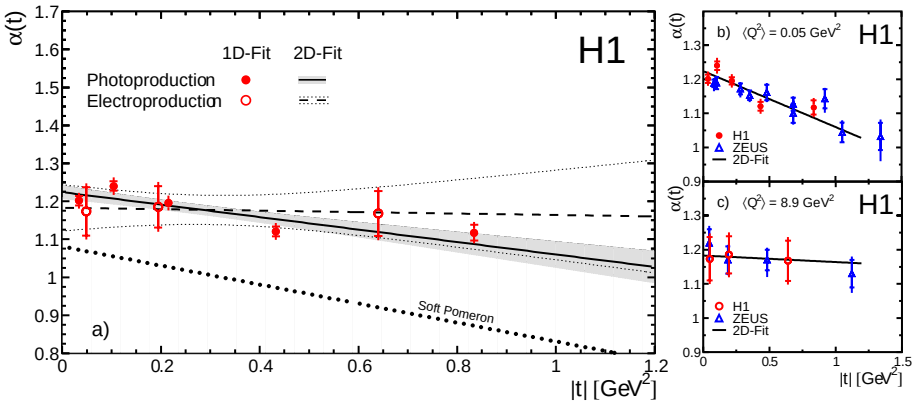

Figure 8: a) Effective trajectory $\alpha(t)$ as a function of $|t|$ for J/ψ photo- ($40 < W < 305$ GeV, $\langle Q^2 \rangle = 0.05$ GeV^2) and electroproduction ($40 < W < 160$ GeV, $\langle Q^2 \rangle = 8.9$ GeV^2). The data points are results of fits to the W dependence of the cross-section in bins of t. The result of a two-dimensional fit with 1σ error contours is also shown. b) and c) show a comparison to ZEUS data [22, 23] for photo- and electroproduction respectively.

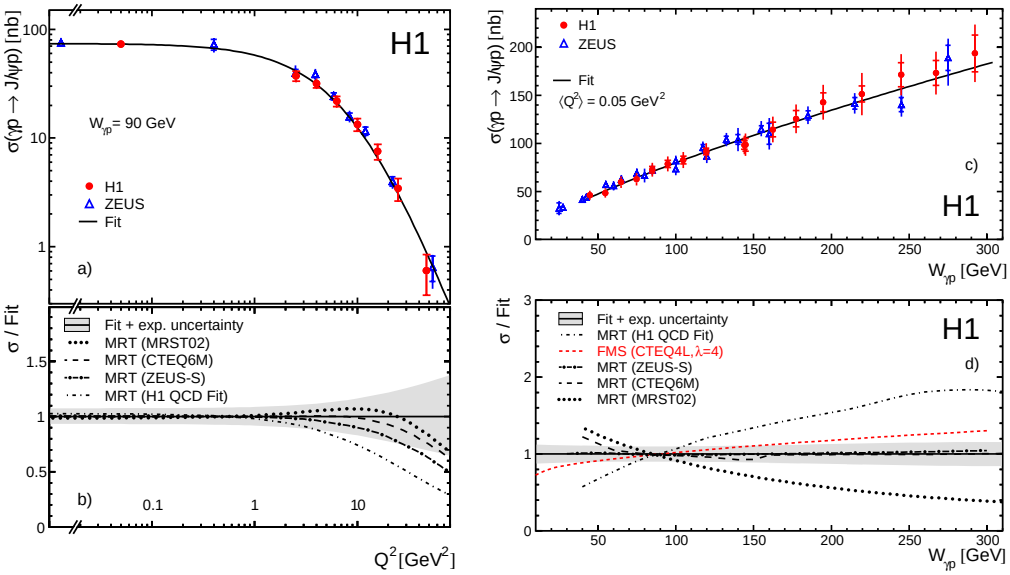

Figure 9: Q^2 and W dependence of the elastic J/ψ cross-section (also showing ZEUS data [22, 23]). The Q^2 dependence (a) is fitted with $\sigma_{\gamma p} \propto (M_\psi^2 + Q^2)^{-n}$. b) shows the ratio of the MRT calculations with different gluon distributions to the fit. The curves are individually normalised to the measurement across the complete Q^2 range, yielding factors between 1.5 and 2.8. c) The W dependence of the cross-section with a fit of the form $\sigma \propto W^\delta$. In d) the ratios of the predictions by the MRT calculation with different gluon distributions and a dipole model (FMS) to the fit are shown. For the MRT curves the normalisation is the same as for the Q^2 distribution whereas the FMS curve is normalised to the fit at $W = 90$ GeV.

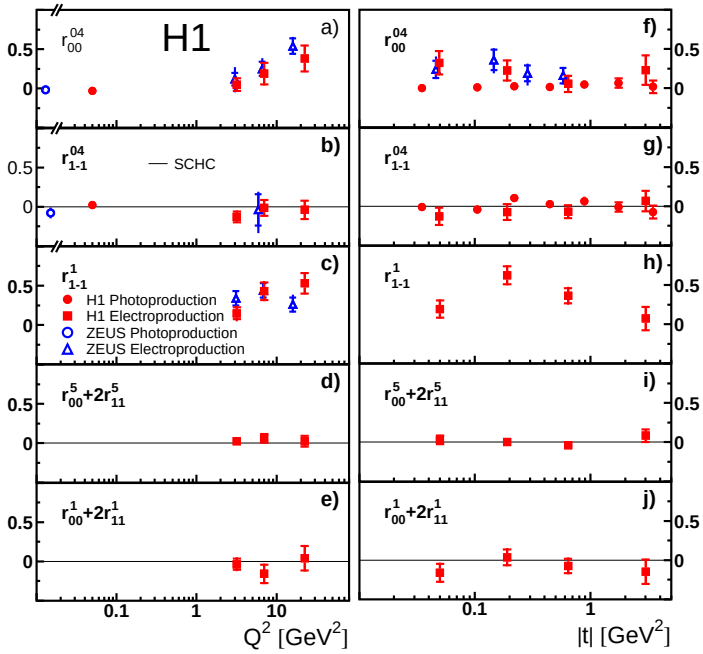

Figure 10: Spin density matrix elements for diffractive J/ψ production as a function of Q^2 (left) and $|t|$ (right). The thin line shows the expectation from SCHC.

showing significant t dependence (shrinkage). In electroproduction, no shrinkage is observed – the trajectory is

$$\alpha_{I\!P}(t) = 1.183 \pm 0.054(stat.) \pm 0.030(syst.) + (0.019 \pm 0.139(stat.) \pm 0.076(syst.))\text{GeV}^{-2} \cdot t.$$

The Q^2 and W dependences of the cross-section can be compared to a pQCD based calculation by Martin, Ryskin and Teuber (MRT, [24, 25]) or a dipole model by Frankfurt, McDermott and Strikman (FMS, [26]). These comparisons (see Figure 9) show a strong sensitivity to the gluon distribution used for the predictions; vector meson measurements thus are sensitive to parton density functions.

A helicity analysis for J/ψ production (here also proton-dissociative events are included), shows no evidence for the violation of s-channel helicity conservation (see Figure 10).

5. Conclusions

Vector meson production at HERA is an excellent laboratory to study the interplay of different scales and the transition from soft to hard regimes. The new H1 measurement of the pomeron trajectory in ρ^0 photoproduction gives a slope $\alpha' = 0.116$ GeV^{-2} – significantly smaller than the value of 0.25 GeV^{-2} obtained from hadron scattering data. At high $|t|$, ρ^0 photoproduction violates s-channel helicity conservation, whilst in J/ψ production the helicity is conserved. Together with improvements in theoretical predictions, the precision of J/ψ cross-section measurements starts to constrain the gluon density in the proton.

The large data sample and the improved triggering capabilities of the H1 experiment at HERA II will provide more high-precision measurements of vector meson production in the coming years.

References

[1] A. Aktas *et al.*, [H1 Collaboration], Eur. Phys. J. **C46** (2005) 585.

[2] A. Aktas *et al.*, [H1 Collaboration], Phys. Lett. **B638** (2006) 422.

[3] A. Baird *et al.*, IEEE Trans. Nucl. Sci. **48** (2001) 1276.

[4] A. Schoning, [H1 Collaboration], Nucl. Instrum. Meth. **A518** (2004) 542.

[5] N. Berger *et al.*, IEEE NSS Conference Record (2004) 1976.

[6] M. Ross and L. Stodolsky, Phys. Rev. **149** (1966) 1172.

[7] P. Söding, Phys. Lett. **19** (1966) 702.

[8] M. Derrick *et al.*, [ZEUS Collaboration], Z. Phys. **C73** (1997) 253.

[9] J. Breitweg *et al.*, [ZEUS Collaboration], Eur. Phys. J. **C2** (1998) 247.

[10] J. Breitweg *et al.*, [ZEUS Collaboration], Eur. Phys. J. **C14** (2000) 213.

[11] D. Aston *et al.*, Nucl. Phys. **B209** (1982) 56.

[12] S. Aid *et al.*, [H1 Collaboration], Nucl. Phys. **B463** (1996) 3.

[13] A. Donnachie and P. V. Landshoff, Phys. Lett. **B296** (1992) 227.

[14] G. A. Jaroszkiewicz and P. V. Landshoff, Phys. Rev. **D10** (1974) 170.

[15] P. V. Landshoff, Nucl. Phys. Proc. Suppl. **12** (1990) 397.

[16] B. List and A. Mastroberardino, DESY-PROC-1999-02 (1998) 396.

[17] R. Weber, Diffractive ρ^0 photproduction at HERA, PhD thesis, ETH Zürich, 2006.

[18] J. D. Jackson, Nuovo Cim. **34** (1964) 1644.

[19] R. Enberg, J. R. Forshaw, L. Motyka and G. Poludniowski, JHEP **09** (2003) 008.

[20] G. G. Poludniowski, R. Enberg, J. R. Forshaw and L. Motyka, JHEP **12** (2003) 002.

[21] S. Chekanov *et al.*, [ZEUS Collaboration], Eur. Phys. J. **C26** (2003) 389.

[22] S. Chekanov *et al.*, [ZEUS Collaboration], Eur. Phys. J. **C24** (2002) 345.

[23] S. Chekanov *et al.*, [ZEUS Collaboration], Nucl. Phys. **B695** (2004) 3.

[24] A. D. Martin and M. G. Ryskin, Phys. Rev. **D57** (1998) 6692.

[25] A. D. Martin, M. G. Ryskin and T. Teubner, Phys. Rev. **D62** (2000) 014022.

[26] L. Frankfurt, M. McDermott and M. Strikman, JHEP **03** (2001) 045.